Published in final edited form as:
Biochemistry. 2013 June 18; 52(24): 4204–4216. doi:10.1021/bi4004414.

A Mutational Analysis of the Active Site Loop Residues in *cis*-3-Chloroacrylic Acid Dehalogenase

Gottfried K. Schroeder, **Jamison P. Huddleston**, **William H. Johnson Jr.**, and **Christian P. Whitman***
Division of Medicinal Chemistry, College of Pharmacy, University of Texas, Austin, TX 78712

Abstract

cis -3-Chloroacrylic acid dehalogenase (*cis*-CaaD) from *Pseudomonas pavonaceae* 170 and a homologue from *Corynebacterium glutamicum* designated Cg10062 share 34% sequence identity (54% similarity). The former catalyzes a key step in a bacterial catabolic pathway for the nematocide 1,3-dichloropropene, whereas the latter has no known biological activity. Although Cg10062 has the six active site residues (Pro-1, His-28, Arg-70, Arg-73, Tyr-103, Glu-114) that are critical for *cis*-CaaD activity, it shows only a low level *cis*-CaaD activity and lacks the specificity of *cis*-CaaD: Cg10062 processes both isomers of 3-chloroacrylate with a preference for the *cis*-isomer. Although the basis for these differences is unknown, a comparison of the crystal structures of the enzymes covalently modified by an adduct resulting from their incubation with the same inhibitor offers a possible explanation. A 6-residue active site loop in *cis*-CaaD shows a strikingly different conformation from that observed in Cg10062: the loop closes down on the active site of *cis*-CaaD, but not on that of Cg10062. In order to examine what this loop might contribute to *cis*-CaaD catalysis and specificity, the residues were changed individually to those found in Cg10062. Subsequent kinetic and mechanistic analysis suggests that the T34A mutant of *cis*-CaaD is more Cg10062-like. The mutant enzyme shows a 4-fold increase in K_m (using *cis*-3-bromoacrylate), but not to the degree observed for Cg10062 (687-fold). The mutation also causes a 4-fold decrease in the burst rate (compared to the wild type *cis*-CaaD), whereas Cg10062 shows no burst rate. More telling is the reaction of the T34A mutant of *cis*-CaaD with the alternate substrate, 2,3-butadienoate. In the presence of $NaBH_4$ and the allene, *cis*-CaaD is completely inactivated after one turnover due to the covalent modification of Pro-1. The same experiment with Cg10062 does not result in the covalent modification of Pro-1. The different outcomes are attributed to covalent catalysis (using Pro-1) followed by hydrolysis of the enamine or imine tautomer in *cis*-CaaD vs direct hydration of the allene to yield acetoacetate in the case of Cg10062. The T34A mutant shows partial inactivation, requiring 5 turnovers of the substrate per monomer, which suggests that the direct hydration route is favored 80% of the time. However, the mutation does not alter the stereochemistry at C-2 of [2-D]acetoacetate when the reaction is carried out in D_2O. Both *cis*-CaaD and the T34 mutant generate (2*R*)-[2-D]acetoacetate, whereas Cg10062 generates mostly the 2*S*-isomer. The combined observations are consistent with a role for the loop region in *cis*-CaaD specificity and catalysis, but the precise role remains to be determined.

cis-3-Chloroacrylic acid dehalogenase (*cis*-CaaD) in *Pseudomonas pavonaceae* 170 is part of a catabolic pathway for the *cis*-isomer of the nematocide 1,3-dichloropropene (**1**, Scheme

*Corresponding author. C.P.W. Tel (512)-471-6198; Fax (512)-232-2606; whitman@austin.utexas.edu.

SUPPORTING INFORMATION

Here we describe ESI-MS results, equations for fitting irreversible inhibition data, conventional analysis results, FitSpace confidence contours and fluorescence titration data for bromide binding, a comparative analysis of both methods, and rapid quench results for Cg10062 and **3**. This material is available free of charge via the Internet at http://pubs.acs.org.

1).[1–3] The enzyme catalyzes the conversion of the *cis*-3-chloro- or 3-bromoacrylate (**2** and **3**, respectively) to malonate semialdehyde (**4**).[4] An enzyme-catalyzed decarboxylation follows to yield acetaldehyde (**5**), which can feed into the Krebs cycle.[5] *cis*-CaaD is a member of the tautomerase superfamily, exhibiting the characteristic β-α-β fold and the catalytic amino-terminal proline.[4,6–8]

Kinetic, mechanistic, mutagenic, and structural studies have delineated the key elements of the mechanism for the *cis*-CaaD-catalyzed reaction (Scheme 2).[4,9–13] In this mechanism, Glu-114 activates a water molecule for attack at C-3 of substrate.[9] The position of Tyr-103 near Glu-114 in the crystal structure suggests that it might assist Glu-114 in the activation of water. Arg-70, Arg-73, and His-28 are proposed to interact with the C-1 carboxylate group (in an unknown manner). This interaction binds the substrate and polarizes the α,β-unsaturated acid to facilitate the addition of water to C-3. Addition of water at C-3 produces the *aci*-carboxylate **6**, which can generate product **4** by one of two plausible routes. In one route, the *aci*-carboxylate collapses and picks up a proton from Pro-1 at C-2 to yield the halohydrin **7** (Scheme 2, route A). Expulsion of the halide results in **4**. Alternatively, **6** can eliminate HX in an α,β-elimination reaction to afford enol **8**, which ketonizes to generate **4** (Scheme 2, route B). Again, Pro-1, functioning as a general acid, provides the proton at C-2. Both routes are possible and thus far, are indistinguishable.

The *Corynebacterium glutamicum* enzyme designated Cg10062 is categorized in the *cis*-CaaD family based on sequence analysis (34% pairwise sequence identity and 54% similarity) and the conservation of Pro-1, His-28, Arg-70, Arg-73, Tyr-103, and Glu-114.[14] Although Cg10062 processes **2** and **3**, it does not convert them to **4** very efficiently (as assessed by the k_{cat}/K_m values).[14–16] The activity might also not be biologically relevant because the surrounding genes do not code for the enzymes in the 1,3-dichloropropene catabolic pathway or homologues of these enzymes. Cg10062 catalyzes the dehalogenation of **2** and **3** with comparable k_{cat} values to those of *cis*-CaaD, but it exhibits very poor substrate affinity, as indicated by the ~10^2-fold increase in the K_m value (using **2**). Moreover, it processes both the *cis* and *trans* isomers of **2**, whereas *cis*-CaaD exhibits a high degree of specificity, completely excluding the *trans*-isomer.

The basis for the differences between Cg10062 and *cis*-CaaD is not known. A comparison of the crystal structures of the "native" forms (bound sulfate or phosphate) for both enzymes does not show any obvious differences in the active site regions or elsewhere.[9,10,12] Indeed, the proteins are very similar and align with an rmsd value of less than 1 Å. However, a comparison of the crystal structures of the two enzymes following their covalent modification at Pro-1 by the adduct resulting from the incubation of enzyme and the irreversible inhibitor, (*R*)-oxirane-2-carboxylate, is much more informative. The native and inhibited structures of Cg10062 do not show significant structural differences (PDB codes 3N4G and 3N4D, respectively).[12] However, an active site 6-residue loop in *cis*-CaaD, (Thr-32 to Phe-37), exhibits a striking shift following covalent modification, adopting a more 'closed' conformation (Figures 1A and B) (PDB codes 3MF8 and 3MF7, respectively).[9,10] Moreover, a pre-steady state kinetic analysis of *cis*-CaaD suggests that substrate binding is accompanied by a concomitant isomerization of the enzyme, which could correspond to the closed state of the enzyme and the movement of the loop.[12] These observations suggest that this loop is flexible and could play a role in the specificity and mechanism of *cis*-CaaD.

In order to determine whether one or more loop residues are responsible for the observed differences in substrate specificity (for **3**) and catalysis, the effects of the individual replacements of six amino acids of the *cis*-CaaD active site loop (Thr-Gly-Thr-Gln-His-Phe) with those of Cg10062 (Ala-His-Ala-Pro-Lys-Tyr) were examined. Steady-state kinetic

parameters and the dissociation constants (K_D) of product bromide, for each mutant, were determined. One mutant (T34A *cis*-CaaD) showed higher K_m (**3**) and K_D (bromide) values. In light of the increased K_m value, additional mechanistic studies were conducted with the T34A mutant of *cis*-CaaD, including pre-steady state burst (rapid quench) experiments with **3** and trapping experiments utilizing an alternative substrate, 2,3-butadienoate (**9**, Scheme 3). A stereochemical analysis of the reaction was also carried out. The results are compared to those obtained with both wild-type *cis*-CaaD and Cg10062. Finally, *in silico* docking studies (Autodock Vina) for substrate **2** with both *cis*-CaaD and Cg10062 were conducted to provide further insight into possible roles of this residue in binding.

EXPERIMENTAL PROCEDURES

Materials

Chemicals, biochemicals, Luria-Bertani (LB) media components, and molecular biology reagents were obtained from sources reported elsewhere,[17,18] or as indicated below. Sodium bromide and sodium phosphate buffer salts were at least 99.99% pure or greater, as indicated by the manufacturer. 2,3-Butadienoate (**9**) was synthesized according to published methods.[19] The DEAE-Sepharose and Phenyl-Sepharose 6 Fast Flow resins used for protein purification were obtained from Sigma-Aldrich Chemical Co (St Louis, MO). The Econo-Column® chromatography columns were obtained from BioRad (Hercules, CA). The Amicon stirred cell concentrators and the YM10 ultrafiltration membranes were purchased from Millipore Corp. (Billerica, MA). Malonate semialdehyde decarboxylase (MSAD) was purified as described previously.[5]

Bacterial Strains, Plasmids, and Growth Conditions

Escherichia coli strain BL21-Gold(DE3) was obtained from Agilent Technologies (Santa Clara, CA). The *E. coli* DH5α cells were obtained from Invitrogen (Carlsbad, CA). The construction of the pET-24a(+) vector containing the gene for *cis*-CaaD and the pET3b vector containing the gene for Cg10062 are described elsewhere.[14,16]

General Methods

Techniques for restriction enzyme digestion, ligation, transformation, and other standard molecular biology manipulations were based on methods described elsewhere.[20] PCR amplifications were conducted in a GeneAmp 2700 thermocycler (Applied Biosystems, Carlsbad, CA). DNA sequencing was performed by the DNA Core Facility in the Institute for Cellular and Molecular Biology (ICMB) at the University of Texas at Austin. Mass spectral data was collected in the ICMB Protein and Metabolite Analysis Facility at the University of Texas at Austin on an LCQ electrospray ion-trap mass spectrometer (Thermo, San Jose, CA). Steady-state kinetic assays were performed on an Agilent 8453 diode-array spectrophotometer at 22 °C. Non-linear regression analysis was performed using the program Grafit (Erithacus Software Ltd., Staines, U.K.). Protein concentrations were determined according to the method of Waddell.[21] Sodium dodecyl sulfate-polyacrylamide gel electrophoresis (SDS-PAGE) was carried out on denaturing gels (12%).[22]

Site-Directed Mutagenesis of cis-CaaD

cis-CaaD mutants were constructed using a pET-24a(+) vector containing the *cis*-CaaD gene as the template. Mutations were introduced with the QuikChange Site-Directed Mutagenesis Kit (Agilent Technologies) following the manufacturer's specifications. Mutagenic oligonucleotide primers (coding and complementary) for the T32A-, G33H-, T34A-, Q35P-, H36K- and F37Y-*cis*-CaaD mutants were obtained from Invitrogen. The forward and reverse primers for these mutants were respectively:

GACGCGCACAGGGGACTGGCTGGAACCCAGCACTTCCTGGCC and GGCCAGGAAGTGCTGGGTTCCAGCCAGTCCCCTGTGCGCGTC for the T32A mutant; GCGCACAGGGGACTGACTCATACCCAGCACTTCCTGGCC and GGCCAGGAAGTGCTGGGTATGAGTCAGTCCCCTGTGCGC for the G33H mutant; GGACTGACTGGAGCCCAGCACTTCC and GGAAGTGCTGGGCTCCAGTCAGTCC for the T34A mutant; GACTGGAACCCCGCACTTCCTGGC and GCCAGGAAGTGCGGGGTTCCAGTC for the Q35P mutant; GGAACCCAGAAAATTCCTGGCCC and GGGCCAGGAATTTCTGGGTTCC for the H36K mutant; and CCCAGCACTACCTGGCCCAGG and CCTGGGCCAGGTAGTGCTGGG for the F37Y mutant. The mutation is underlined in each primer. The DNA products were purified using the MinElute PCR Purification Kit (Qiagen, Valencia, CA) and transformed into *E. coli* DH5α cells for plasmid preparation. Single colonies were used to inoculate 20 mL of LB media containing kanamycin (30 μg/mL). The cultures were grown overnight at 37 °C and plasmids were isolated using the GenElute Plasmid Miniprep Kit (Sigma-Aldrich).

Expression and Purification of cis-CaaD Mutants

Plasmids containing the genes for the *cis*-CaaD mutants were transformed into *E. coli* BL21-Gold (DE3) competent cells. LB media (2 L) containing kanamycin (30 μg/mL) was inoculated using ~24 mL of an overnight culture (37 °C) from a single colony and incubated for ~2 h at 37 °C. Protein expression was induced with isopropyl-β-D-thiogalactoside (1 mM, final concentration), followed by a 4 h induction period (37 °C). Cells were harvested by centrifugation (4,000 × g), with yields ranging from 3.5–5.5 g, and stored overnight at −80 °C. Cells were suspended in 10 mM Na_2HPO_4 buffer, pH 8 (Buffer A), and lysed by sonication.[4] The resulting solution was centrifuged for 30 min (23,500 × g) and the supernatant was subjected to an additional 30 min of centrifugation (330,000 × g). The clarified supernatant was filtered (0.2 μM pore) and loaded onto a DEAE-Sepharose column (1 × 10 cm, ~8 mL resin) pre-equilibrated with Buffer A. The column was washed (~1 mL/min) with 20 mL of Buffer A followed by a linear salt gradient (0–0.5 M Na_2SO_4, 100 mL). Protein typically elutes from 18–30 min after initiation of the salt gradient. Protein purity in the individual fractions was evaluated by SDS-PAGE and activity assays. Fractions with the highest purity and activity were pooled and $(NH_4)_2SO_4$ (1 M final concentration) was added. After the resulting solution stirred on ice for 1 h, it was filtered (0.2 μM pore) and loaded onto a Phenyl-Sepharose 6 Fast Flow column (0.5 × 10 cm, ~3.5 mL resin) pre-equilibrated with Buffer A containing 1 M $(NH_4)_2SO_4$ (Buffer B). The column was washed with Buffer B to elute the remaining protein. Protein typically elutes during sample loading (after two column volumes) with the highest protein concentrations in the next four fractions (2 mL each). The appropriate fractions were pooled, exchanged into Buffer A, concentrated to ~20 mg/mL using an Amicon concentrator (10,000 MW cutoff), and stored at 4 °C. Yields were typically ~150 mg of pure protein from 2 L of culture. The molecular masses of the mutant proteins were also determined by mass spectral analysis and are reported in Supporting Information Table S1, along with the calculated masses.

Expression and Purification of Cg10062

The pET3b vector containing the gene for Cg10062 was transformed into *E. coli* BL21-Gold (DE3) competent cells. LB media (2 L) containing ampicillin (100 μg/mL) was inoculated using ~24 mL of an overnight culture (37 °C) from a single colony and incubated for ~8 h at 37 °C. Cells were harvested by centrifugation (4,000 × g), with a yield of 10.5 g, and stored overnight at −80 °C. Cell lysis and protein purification were carried out using the procedures described above for the *cis*-CaaD mutants, with the following modifications. The pooled fractions from the DEAE column purification were treated with $(NH_4)_2SO_4$ (1.5 M) and the phenyl column was pre-equilibrated with Buffer A containing 1.5 M $(NH_4)_2SO_4$ (Buffer C).

After protein loading, the column was washed with 10 mL of Buffer C. Protein typically elutes during sample loading (after three column volumes) with the highest protein concentrations in next four fractions (2 mL each). The appropriate fractions were pooled, exchanged into Buffer A, concentrated to ~19 mg/mL using an Amicon concentrator (10,000 MW cutoff), and stored at 4 °C. The purification yielded ~100–300 mg of pure protein from 2 L of culture. Typically, the molecular subunit mass ranged from 17,098.0–17100.0 Da (calc, 17097.2 Da), which is within experimental error of those found previously.[14,15]

Steady-State Kinetic Parameters

Purified proteins were exchanged into 100 mM Na_2HPO_4 buffer, pH 8, using an Amicon concentrator (10,000 MW cutoff) for kinetic analysis. For all steady-state assays, protein was diluted to 2 μM (based on monomer mass) and allowed to equilibrate for ~1 h. Stocks of *cis*-3-bromoacrylic acid (**3**, 20 mM or 50 mM) were made using appropriate ratios of dibasic (100 mM) and tribasic (100 mM) phosphate buffer to a final pH of 8. Assays (1 mL) were initiated by the addition of 0–12 μL of a concentrated stock solution (0–500 μM, final concentration). The decrease in UV absorbance (ε_{224} = 3,600 M^{-1} cm^{-1}) was monitored for the first 40 s of reaction. Initial rates were determined from the first 16 s of reaction, plotted versus substrate concentration, and fit to the Michaelis-Menten equation to calculate the steady-state parameters k_{cat} and K_M. The full kinetic time course was also monitored over a 5 min period (data not shown).

The steady-state kinetic rate parameters for the T32A (1.4 μM, final concentration) and T34A (0.2 μM, final concentration) mutants of *cis*-CaaD were determined using a coupled assay[14,15] containing MSAD, aldehyde dehydrogenase, and NAD^+. Assays (1 mL) were run in 100 mM phosphate buffer at pH 8 (22 °C) using various concentrations of **3** (0–10,000 μM). Steady-state kinetic parameters for Cg10062 (2 μM) with **3** were also determined using a coupled assay containing MSAD (0.07 mg, 4 μL of 18 mg/mL), alcohol dehydrogenase (0.12 mg, 20 μL of 6 mg/mL stock solution), and NADH (160 μM, 20 μL of 6 mg/mL stock solution, ε_{340} = 6,220 $M^{-1}cm^{-1}$) in 100 mM phosphate buffer at pH 8.

The steady-state kinetic parameters for Cg10062 (0.175 μM, final concentration) and the T34A mutant of *cis*-CaaD (1.6 μM, final concentration) with 2,3-butadienoate (**9**) were determined (100 mM phosphate buffer, pH 8), by following the decrease in UV absorbance at 224 nm (ε_{224} = 1125 $M^{-1}cm^{-1}$)[13] or 255 nm (ε_{255} = 160 $M^{-1}cm^{-1}$), respectively. Because the T34A mutant of *cis*-CaaD has a higher K_m value using **9**, the reaction was followed at 255 nm where the absorbance of **9** maintained linearity at higher concentrations.

Determination of the Bromide Dissociation Constants (K_D)

Stopped-flow fluorescence experiments were previously carried out using the intrinsic protein fluorescence of *cis*-CaaD to monitor pre-steady-state substrate turnover.[12] Here, the change in enzyme fluorescence was monitored (1 s duration) as a function of increasing product bromide concentration in phosphate buffer (100 mM) at pH 8. Enzyme (20 μM before mixing, equilibrated 1 h) and NaBr solutions (0–100 mM before mixing) were mixed in a 1:1 ratio in the stopped-flow instrument (1.3 ms dead time). All experiments were conducted on a SF 2004 series stopped-flow apparatus (Kintek Corp, Austin, TX) at 22 °C. The fluorescence was excited at 280 nm with the monochromator and light filter slit widths set at 0.28 mm. Emission was observed using a 340 nm band pass filter (Semrock, Rochester, NY). Fluorescent traces represent an average of at least 5 individual runs (1000 data points each). To determine the dissociation constant (K_D) for bromide, the steady-state fluorescence endpoints of each transient were plotted versus bromide concentration [X] and fit to (eq 1), where F is the observed fluorescence, F_0 is the initial fluorescence, and ΔF is

the total change in fluorescence intensity. The stopped-flow data was also fit by simulation with KinTek Explorer[23] using the fitted constants from eq 1 as constraints.

$$F = F_0 + \Delta F \left(\frac{[X]}{K_D + [X]} \right) \quad \text{eq 1}$$

The bromide dissociation constant for wild-type *cis*-CaaD was also determined by equilibrium fluorescence titration using the TMX-1000 Titration Module on the SF 2004 series stopped-flow apparatus (Kintek Corp) at 22 °C. A 100 mM bromide solution was slowly added (0.035 mL total) from a 0.05 mL Hamilton syringe to 0.24 mL of a stirred solution containing *cis*-CaaD (10 mM) over 5 min. All solutions were made up in 100 mM phosphate buffer at pH 8. The experiment was repeated 5 times, each trace was fit to eq 1, and the fitted parameter values were averaged.

Rapid-Quench Experiments

Rapid quench experiments (22 °C) were conducted in phosphate buffer (100 mM, pH 8) on a KinTek RQF-3 Rapid Quench Flow apparatus, according to previously published methods.[12] In brief, excess substrate **3** (10 mM after mixing) was mixed in a 1:1 ratio with enzyme (0.125 and 0.15 mM after mixing for wild-type and T34A *cis*-CaaD, respectively) and the reaction was quenched with H_2SO_4 (0.6 M) after varying periods of time (0.006–1.5 s). A minimum of 25 time points was collected for each experiment. Additional rapid quench experiments were also conducted with Cg10062 (0.5 mM after mixing) and **3** (10 mM after mixing) at 15 different time points between 0.1–2.4 s. Product bromide concentrations were determined by ion chromatography (IC) on an ICS-1500 ion chromatography system (Dionex Corp, Bannockburn, IL), as described previously.[12] The data were fit to the burst equation (eq 2),

$$[P]_{obs} = Ae^{-\lambda t} + k_{ss}t + C \quad \text{eq 2}$$

where $[P]_{obs}$ is the observed concentration of product bromide, A is the burst amplitude (A_0) multiplied by the active enzyme concentration ($[E]_0$), λ is the burst rate constant, k_{ss} is the steady state turnover rate (which approaches k_{cat} at saturating substrate concentration) multiplied by the active enzyme concentration ($[E]_0$), and C is a constant.[12,24]

Stereochemical Analysis of [2-D]10

The stereochemical analysis of [2-D]acetoacetate ([2-D]**10**), generated by the reaction of Cg10062 or the T34A mutant of *cis*-CaaD with 2,3-butadienoate (**9**), was carried out as described previously for *cis*-CaaD,[13] with the following modifications. A solution of **9** (40 mg, 0.48 mmol), dissolved in 100 mM Na_3PO_4 buffer made up in D_2O, was processed as described to exchange protons with deuterons. The resulting residue was dissolved in 2 mL of D_2O to generate a stock solution. A 200-μL aliquot of this solution was mixed with a 200-μL aliquot of a 100 mM Na_2DPO_4 buffer solution (in D_2O) in order to maintain a neutral pH. The mixture was then combined with 200 μL of enzyme solution (Cg10062 or the T34A mutant of *cis*-CaaD), previously exchanged in D_2O. The final concentrations were as follows: allene **9** (4 mg, 79.4 mM); Cg10062 (0.14 mM); and T34A-*cis*-CaaD (0.37 mM). A total of five reactions mixtures were made for each enzyme. After 3 min, a 50-μL aliquot of $NaBH_4$ (2.6 M solution made up in D_2O) was added to the individual reaction mixtures. The procedure then followed the one used for the stereochemical analysis of *cis*-CaaD.[13] Accordingly, the diastereomeric mixture of the corresponding alcohol [2-D]-3-hydroxybutyate (**11**) was recovered by anion exchange chromatography, and the 3*R*-isomer

of [2-D]**11** was removed by enzymatic means (D-β-hydroxybutyrate dehydrogenase and acetoacetate decarboxylase). The remaining isomer, (3*S*)-[2-D]**11**, was isolated and analyzed by ^{1}H NMR spectroscopy. Comparison to the known spectra for (2*S*,3*S*)- or (2*R*, 3*S*)-[2-D]**11** was used to assign the stereochemistry at C-2 of [2-D]**10**.[13]

The Reaction of the T34A Mutant of cis-CaaD with 9 and $NaCNBH_3$

Reaction mixtures (100 μL) contained $NaCNBH_3$ (20 μL of a 1.6 M stock solution in 100 mM Na_2HPO_4 buffer, pH 8) and the T34A mutant of *cis*-CaaD (30 μL of a 0.34 mM stock solution, 0.56 mg total) in 100 mM Na_2HPO_4 buffer (pH 8). The addition of varying amounts of **9** (0–50 μL of a 10 mM stock solution in 100 mM Na_2HPO_4 buffer, pH 8) initiated the reactions. To ensure reaction completion, the mixtures were incubated overnight and the remaining enzymatic activity was determined using **2**, as described previously.[13] Assay mixtures (1 mL) contained 5 μL of the incubation mixture and 10 μL of **2** (100 mM, made up in 100 mM phosphate buffer, pH 8). Initial rates for substrate loss (ε_{224} = 3600 $M^{-1}cm^{-1}$), monitored for increasing periods of time (1–15 min) depending on the amount of **9**, were determined (in triplicate) by linear regression. The number of equivalents of **9** required for complete inhibition was estimated by fitting a plot of % activity versus equivalents of **9** (per enzyme monomer) to a modified form of the quadratic equation (Supporting Information Text S1).

The number of equivalents of **9** processed by the T34A mutant of *cis*-CaaD prior to complete inhibition in the presence of $NaBH_4$ was also determined by ^{1}H NMR spectroscopy. A 10 mL solution of T34A *cis*-CaaD (780 μM based on the monomer molecular mass, 130 mg total) was exchanged into 10 mM phosphate buffer (pH 8) using an Amicon concentrator (10,000 MW cutoff). This process was repeated five times. An aliquot (66.7 μL) of a $NaBH_4$ stock solution (2.6 M made up in 100 mM phosphate buffer, pH 8) was added to the enzyme solution followed by a 5-min incubation period. A total of 0.6 mL of a stock solution containing **9** (79.4 mM made up in 100 mM phosphate buffer, pH 8) was then added to the reaction mixture in 100 μL aliquots (with stirring) over 2 min (4760 μM final concentration). The enzymatic activity of the solution was monitored using 1 μL aliquots (using the assay described above) until less then 5% activity remained. The enzyme was removed by filtration (Amicon concentrator, 10,000 MW cutoff) and the filtrate was evaporated to dryness. The resulting sample was reconstituted with D_2O and evaporated to dryness. This process was repeated three times to completely exchange the sample into D_2O. The ^{1}H NMR spectrum (400 MHz) was obtained in D_2O and the final ratio of **11** (from the reduction of **10** to the alcohol **11**)[13] to remaining starting material (**9**) was determined. Control experiments containing **9** alone under identical conditions did not show the presence of any alcohol, **11**, (or **10**), by ^{1}H NMR spectroscopy, following an overnight incubation period. Additional control experiments with wild-type *cis*-CaaD and **9** (identical conditions) were also conducted as described above.

In Silico Docking Studies

Docking studies were performed using Autodock Vina[25] and PyMOL[26] version 1.2 with an Autodock plugin[27] for PyMOL, an interface (developed on Linux) which utilizes MGLTools Version 1.5.4 and NumPy version 1.3. The crystal structures for *cis*-CaaD and Cg10062 (PDB codes 2FLZ and 3N4G, respectively) were used as rigid receptors, following the removal of all water molecules. A structural alignment of both receptors was executed in PyMOL. The computer program Marvin (ver. 5.4.1.1, 2010, ChemAxon, http://www.chemaxon.com) was used to generate the flexible ligand, *cis*-3-chloroacrylate (**2**), in the mol2 (3D) file format. Search space for docking was a 15 Å box centered about the Pro-1 residue of each active site. In addition to the energy scoring function of Vina, results were evaluated by goodness-of-fit of the docked ligand within the active site volume.

RESULTS

Loop Analysis

The 6-residue loop in *cis*-CaaD connects the α-helix (α) and the second β-sheet (β2) of the tautomerase superfamily common β-α-β building block.[9] A sequence alignment of *cis*-CaaD and Cg10062 (first two entries, Figure 2) shows high sequence conservation in the leading helix (α) and the trailing β-sheet (β2), but no common amino acids in the loop region (boxed area, Figure 2). A BLAST search using the *cis*-CaaD sequence identified several additional putative family members,[28] with representative sequences (from different species) for the most significant hits shown in Figure 2. A comparison of the loop region sequences (shaded portion) indicates that Ala-32 and His-33 in Cg10062 and Thr-34 and Gln-35 in *cis*-CaaD appear unique to these two enzymes. Moreover, the otherwise strict conservation of a proline residue at position 35 (caret, Figure 2) extends throughout the tautomerase superfamily, including *trans*-3-chloroacrylic acid dehalogenase (CaaD),[29,30] 4-oxalocrotonate tautomerase (4-OT),[31] macrophage migration inhibitory factor (MIF),[32] 5-(carboxymethyl)-2-hydroxymuconate isomerase (CHMI),[31] and MSAD.[5] In addition, a structural alignment of the apo forms of *cis*-CaaD and Cg10062 reveals that the backbone traces of the two loop regions are very similar, with only a slight deviation near residues 32 and 33 (Figure 3A). This may reflect the fact that the side chain hydroxyl moiety of Thr-32 in *cis*-CaaD is within hydrogen bond distance of the backbone carbonyl of His-28.

Steady-State Kinetic Parameters Using 3

The steady-state kinetic parameters (with **3**) for wild-type *cis*-CaaD, the corresponding loop mutants, and Cg10062 are summarized in Table 1 and graphically in Figure 3B. On this basis, the most significantly impaired mutants compared with wild-type are the T32A and T34A mutants. The value of K_m increases ~19-fold for the T32A mutant and ~4-fold for the T34A mutant, whereas the k_{cat} values decrease by ~3- and 1.4-fold, respectively. The k_{cat} and K_m values for the Q35P mutant were also significantly altered (reduced by ~9- and ~10-fold, respectively), but the overall efficiency is comparable to that of wild type (as assessed by the k_{cat}/K_m values).

Bromide Dissociation Constant (K_D)

The addition of bromide (*P*) to free enzyme (*E*) resulted in the formation of a new enzyme state with reduced fluorescence intensity (*FP*). The dissociation constants for wild-type *cis*-CaaD, the corresponding loop mutants, and Cg10062 are reported in Table 1 and represented graphically in Figure 3B (light gray). Binding of bromide was weaker for the T32A, G33H, T34A and H36K mutants of *cis*-CaaD, whereas both the Q35P and F37Y mutants of *cis*-CaaD exhibited stronger affinity for bromide. Interestingly, Cg10062 exhibits an equivalent K_D value for bromide (versus *cis*-CaaD), but with a significantly reduced (6-fold) ΔF value (Table 1). The stopped-flow data for wild-type *cis*-CaaD and bromide (Figure 4A) and a plot of the corresponding steady-state fluorescence endpoints (shaded area) versus bromide concentration (Figure 4B, fit to eq 1, solid line) are shown in Figure 4. The stopped-flow traces are characterized by a rapid initial decrease in fluorescence (faster than the instrument dead time of 1.3 ms), indicative of a rapid equilibrium binding event. In addition, the traces begin to exhibit some curvature as the bromide concentration is increased, although this effect is not significantly expressed with low amounts of bromide. A similar trend was observed for each of the loop mutant enzymes, except for the T32A mutant, which did not exhibit any initial curvature (data not shown). The data was also fit by simulation (KinTek Explorer) to Scheme 4 (Figure 4A, solid lines), where *E* is enzyme, *F* is a second fluorescent form of the enzyme, and *P* is product bromide. Development of the final simple model shown in Scheme 4 was guided by conventional analysis, utilizing a fit of each kinetic trace to a single exponential and plotting the resulting amplitude versus bromide concentration

(Supporting Information Figure S1) and the first order rate constants versus bromide concentration (data not shown). The concentration dependence of both terms exhibited an initial lag phase, consistent with the increase in curvature observed in the raw kinetic traces as a function of increasing bromide concentration. All attempts to fit the data by simulation using models incorporating a direct isomerization step following an initial binding event (i.e., $E + P = EP = EP^*$) were unsuccessful (data not shown), predicting excessive curvature at low bromide concentrations. Moreover, such models do not predict any lag in the concentration dependence of the amplitude or rate terms resulting from fitting to a single exponential, as is observed for the data. To account for the observed non-linear dependence, we propose that the enzyme exhibits a weak affinity (K_2) for a second molecule of bromide and used the model shown in Scheme 4 to successfully fit the data (Figure 4A, solid lines). Subjecting the simulated traces to conventional analysis yielded results very similar to those observed for the raw data (Supporting Information Figure S1). Therefore, the kinetic model shown in Scheme 4 represents the simplest model that completely accounts for all of the data.

Due to the relatively small overall amplitude of the second step, FitSpace analysis indicated that the values for the individual parameters k_2 and k_{-2} were not as well resolved.[33] However, reliable upper and lower limits for the equilibrium constant could be determined (K_2 = 5–10 mM). The fitted value for the initial equilibrium step (K_1 = 3700 s^{-1}) was well constrained, with upper and lower limits of 3800 s^{-1} and 3300 s^{-1}, respectively (threshold limit at 5% of the lowest sum squared error (SSE) for the best fit). The results of the FitSpace analysis can be found in Supporting Information Figure S2.

The K_D for bromide binding to wild-type *cis*-CaaD was also determined by equilibrium fluorescence titration as 3900 ± 170 μM (Supporting Information Figure S3, fit to eq 1 shown as solid line). This value is within experimental error of both values determined using steady-state fluorescence endpoints (3700 ± 200 μM) or direct data fitting by simulation, as described above. The total change in fluorescence intensity (ΔF) determined by this method was −1.4 (± 0.06), somewhat higher than that observed by endpoint fluorescence (ΔF = −1.8 ± 0.05, see Supporting Information Text S2).

Rapid Quench Experiments

The results of the rapid quench experiments for the reaction of **3** (10 mM after mixing) with both wild-type (0.125 mM after mixing) and the T34A (0.15 mM after mixing) mutant of *cis*-CaaD are shown in Figures 5A and 5B, respectively. A pre-steady state burst of product (bromide) formation was observed with wild-type *cis*-CaaD (Figure 5A). Fitting the data to eq 2 yielded a burst rate (λ) of 12 ± 2 s^{-1} and a calculated steady-state turnover rate of 6 ± 0.5 s^{-1}, somewhat faster than that determined for k_{cat} by the UV assay (4.3 s^{-1}). For the T34A mutant of *cis*-CaaD, a relatively modest burst in product (bromide) formation was observed (Figure 5B). Fitting the data to eq 2 yielded a burst rate (λ) of only 3 ± 1 s^{-1} and a calculated steady-state turnover rate of 8 ± 0.5 s^{-1}. As observed with the wild-type enzyme, the calculated steady-state turnover rate is faster than that determined for k_{cat} by the UV assay (3 s^{-1}). For comparative purposes, experiments with Cg10062 (0.5 mM after mixing) and **3** (10 mM after mixing) were also conducted (Supporting Information Figure S4). Under these conditions, there was no evidence for a pre-steady state burst of product formation, but only the linear production of bromide as a function of time (0.1–2.4 s).

Steady-State Kinetic Parameters Using 9

The steady-state kinetic parameters (with **9**) for wild-type *cis*-CaaD, T34A-*cis*-CaaD, and Cg10062 are reported in Table 2. Within experimental error, the kinetic parameters for Cg10062 and *cis*-CaaD are comparable. The T34A mutant of *cis*-CaaD shows a ~11-fold

increase in K_m and a slight increase in k_{cat}, to give an ~8-fold decrease in the k_{cat}/K_m value (compared to wild type *cis*-CaaD).

Stereochemical Assignment at C-2 of 10 in the Cg10062- and T34A-cis-CaaD-catalyzed Reactions

The stereochemical analysis of [2-D]**10**, generated in the Cg10062- or T34A-*cis*-CaaD-catalyzed reaction with **9** in D_2O, relies on the diastereotopic nature of the C-2 protons in (3*S*)-**11** (Scheme 3).[13] Each diastereotopic proton at C-2 of (3*S*)-**11** gives a doublet of doublets centered at ~2.17 ppm and ~2.28 ppm in a ^{1}H NMR spectrum (Figure 6A).[13] The ^{1}H NMR spectrum of (2*S*,3*S*)-[2-D]**11**, isolated as described,[13] is shown in Figure 6B. The ^{1}H NMR spectrum of (2*R*,3*S*)-[2-D]**11**, generated in the reaction of *cis*-CaaD with **9** and the subsequent degradation,[13] is shown in Figure 6C. The (2*R*,3*S*)-isomer of [2-D]**11** is favored by a ratio of 5:1. The ^{1}H NMR spectrum of (3*S*)-[2-D]**11**, isolated from the reaction of T34A-*cis*-CaaD and **9** in D_2O and subsequent degradation, is shown in Figure 6D. Clearly, the (2*R*,3*S*)-[2-D]**11** isomer has been isolated indicating that the stereochemistry at C-2 of [2-D]**10** is *R*. Although the (2*R*,3*S*)-[2-D]**11** isomer appears to be the sole product of the reaction, this is likely due to the shorter incubation time (3 min for the T34A mutant vs 5 min for *cis*-CaaD[13]). The longer incubation time allows for exchange of the acidic C-2 protons. Finally, the ^{1}H NMR spectrum of (3*S*)-[2-D]**11**, isolated from the reaction of Cg10062 and **9** in D_2O and subsequent degradation, is shown in Figure 6E. In this reaction, the (2*S*,3*S*)-[2-D]**11** isomer is the predominant product isolated indicating that the stereochemistry at C-2 of [2-D]**10** is *S*. The (2*S*,3*S*)-[2-D]**11** isomer is favored by a ratio of 4:1. (It is not clear if this ratio has mechanistic significance or if it results from the reaction conditions.) In summary, *cis*-CaaD and the T34A mutant generate the same isomer of [2-D]**10**, whereas Cg10062 yields the opposite one.

Inhibition of the T34A mutant of cis-CaaD by 9 in the Presence of $NaCNBH_3$

The T34A mutant of *cis*-CaaD (0.56 mg) was incubated with **9** in the presence of $NaCNBH_3$ in order to determine the number of equivalents of **9** required for complete inactivation of the enzyme. The % activity of the enzyme decreases as a function of an increasing number of equivalents of **9** (per monomer) (Figure 7). The data is fit (solid line) to a modified form of the quadratic equation (eq S1), assuming infinitely tight (irreversible) binding. This analysis (see Supporting Information Text S1) indicates that the number of equivalents of **9** required for complete inhibition (i.e., covalent modification of Pro-1) is 5 ± 0.2 equivalents per monomer. These results are consistent with the predominate attack of water, as opposed to the exclusive direct attack of **9** by Pro-1.[13]

The number of equivalents of **9** processed by the T34A mutant of *cis*-CaaD in the presence of $NaCNBH_3$ was also determined by ^{1}H NMR spectroscopy, via peak intergration of the signals corresponding to the substrate (**9**, Scheme 3) and reduced product (**11**).[13] This experiment yielded identical results to those of the inhibition experiments (i.e., 5 equivalents per monomer).

In Silico Docking Studies

Docking results representing the best fit (lowest energy binding orientation) for **2** to *cis*-CaaD and Cg10062 are shown in Figures 8A and 8B, respectively. The estimated binding affinity[25] for **2** to *cis*-CaaD and Cg10062 was −3.9 and −2.0 kcal/mol, respectively. In addition, both docked ligands (space-filling model) fit within the active site volume of each enzyme, as represented by the mesh surfaces (gray) shown in Figure 8. Moreover, **2** docked to both enzymes in vary similar orientations (best fit), with the C3 atom (of **2**) in close

proximity (~3 Å) to the nitrogen atom of the active site Pro1 residue and near the putative bound water molecule required for hydration.

DISCUSSION

Active site loops are well known to play critical roles in enzyme catalysis and substrate specificity.[34] The role of the so-called phosphodianion gripper loop in catalysis in triose phosphate isomerase (TIM), orotidine 5′-monophosphate decarboxylase (OMPDC), and glycerol 3-phosphate dehydrogenase has been studied intensely.[33–35] Binding of the substrate phosphate dianion drives a conformational change that closes the loop over the substrate, thereby sequestering it from solvent. The reduced active site dielectric constant and other associated conformational changes resulting from loop closure contribute to the catalysis of the specific reaction. In the enolase enzyme superfamily, two loops largely define substrate specificity. These loops (designated the 20s and 50s loops) are in the capping domain, which along with a modified TIM barrel domain, comprise the two-domain structure of all enolase superfamily members.[36–39] The catalytic components for the generation, stabilization, and processing of an enediolate species, the characteristic partial reaction of the superfamily, are conserved (or "hard-wired")[39] in the core scaffolding, (i.e., the TIM barrel domain). The capping domain loops define the volume, shape, and polarity of the cavity, which, in turn, determine the substrate specificity. Similar examples where loops serve as substrate recognition elements have been described for the members of the haloalkanoic acid dehalogenase (HAD) enzyme superfamily.[40]

In this context, the conformation adopted by the loop region (residues 32–37) in the "inhibited" structure of *cis*-CaaD (Figure 1B) and the absence of a similar conformation in "inhibited" structure of Cg10062 suggest that this loop might play a role in the specificity and/or mechanism of *cis*-CaaD. It appears that the loop is sufficiently flexible to adopt a new conformation following covalent modification of the active site with an inhibitor, whereas the same modification to Cg10062 has no structural effect. If a similar event occurs upon substrate binding, it might account for some of the differences between *cis*-CaaD and Cg10062, and identify a new component of *cis*-CaaD specificity and/or catalysis.

Accordingly, each loop residue of *cis*-CaaD was replaced with the corresponding one in Cg10062 to probe the potential role of these residues in specificity and catalysis. These replacements, rather than alanine substitutions, assess the differences between Cg10062 and *cis*-CaaD directly and, as such, better mimic the changes that might result from natural (or directed) selection. Moreover, each change is evaluated on an individual basis, which, given the relatively slight thermodynamic favorability of the folded state minimizes the potential loss of stability that might occur with a swap of the entire 6-residue loop.[41,42] The highly analogous orientations of the amino acid backbones of both loop regions (Figure 3A) also render it less likely that significant structural perturbations will be introduced at the active site.

On the basis of sequence and structural analysis, the T32A, G33H, Q35P and T34A *cis*-CaaD mutants appear to be the most likely candidates for possible roles in substrate specificity and/or catalysis because each represents a unique substitution of a highly conserved residue in the *cis*-CaaD family (Figure 2). The most stringently conserved residue is Pro-35, which is replaced with Gln-35 in *cis*-CaaD. The presence of the rigid proline residue in this position in Cg10062 could partially explain the apparent lack of loop movement in the enzyme following covalent inhibition.[12] Mutations that reduce loop flexibility could potentially impede optimization of enzyme-substrate interactions in both the ground state and the transition state, thereby reducing the rates of substrate binding and

chemistry. Such rigidity could also dampen product release rates, as relaxation of the loop may be less thermodynamically favored.

A graphical summary of the steady state kinetic parameters for all of the active site loop mutants of *cis*-CaaD is shown in Figure 3B. Each mutation, except the G33H, reduces the value of k_{cat}. Mutations of the first three loop residues (32–34) increase the K_m value, whereas mutations of the following three residues (35–37) decrease the K_m value. Parallel changes in the K_D for bromide were also observed. In general, mutations of residues 32–34, which are near the putative binding site for the carboxylate moiety of the substrate (i.e., His-28, Arg-70, and Arg-73) decrease the bromide affinity (Figure 3B, Table 1). In contrast, both the Q35P and F37Y mutants of *cis*-CaaD (located closer to Glu-114 and Tyr-103 in the putative halide binding pocket) exhibit an increase in bromide affinity (Figure 3B, Table 1). These differences might reflect alterations in loop mobility and/or the polarity of the putative halide binding pocket.

Steady-state kinetic analysis of the Q35P mutant of *cis*-CaaD shows a ~10-fold reduction in both k_{cat} and K_m (vs the wild-type enzyme). At first glance, the reduction suggests that substrate binding is more favorable, which is at odds with the preceding sequence and structural analysis, and the expectation that this mutant of *cis*-CaaD would be more Cg10062-like. However, K_m is a composite of many rate constants, and as such, is difficult to interpret.[24] Additional transient state experiments combined with global fitting of all kinetic data (stopped-flow, rapid quench, and steady state) to a single mechanism can resolve the rate constant for each kinetically significant step.[13,23] The effect of the Q35P mutant on the various steps of the reaction (e.g., binding, chemistry, conformational changes, and/or product release) can then be more critically evaluated. The appropriate experiments for the Q35P mutant of *cis*-CaaD are underway.

Both the T32A and T34A mutants of *cis*-CaaD show higher K_m values versus wild-type *cis*-CaaD, as does Cg10062 (although not to the same extent). To determine whether the higher K_m values reflect a more “Cg10062-like” *cis*-CaaD mutant, additional kinetic and mechanistic experiments were carried out on the T34A mutant and compared with those performed on Cg10062. (The T32A mutant showed the highest K_m value using **3**, but mechanistic experiments with the alternative substrate **9** are not feasible because the corresponding K_m for **9** is too high to achieve saturating concentrations.)

First, a pre-steady state kinetic analysis was carried out with the T34A mutant of *cis*-CaaD. The enzyme showed a relatively modest pre-steady state burst of bromide formation versus that of wild-type enzyme (Figure 5), and corresponded to a 4-fold reduction in the fitted burst rate ($\lambda = 3 \pm 1\ s^{-1}$), potentially reflecting a shift in mechanism or the nature of the rate limiting step. Rapid quench experiments conducted with Cg10062 and **3** did not exhibit any pre-steady state burst in bromide production (Figure S4). Although this result should be interpreted cautiously because the observed linearity could, in part, reflect difficulties in achieving saturating substrate concentrations, it appears that the T34A mutant of *cis*-CaaD is more Cg10062-like, in this respect.

The second set of experiments involves reactions with the alternate substrate **9**. In the course of a previously reported stereochemical analysis of *cis*-CaaD with **9**, an alternative mechanism to the one shown in Scheme 2 was implicated.[13] In this analysis to determine the overall stereochemical course of the *cis*-CaaD-catalyzed reaction using **2** and **3** (syn vs anti), a strategy was pursued where **9** and substituted chiral allenes would be incubated with the enzyme in presence of $NaBH_4$. For **9**, it was anticipated that the presence of the $NaBH_4$ would trap the labeled acetoacetate, [2-D]**10** (Scheme 3), as the labeled 3-hydroxybutyrate, [2-D]**11**. Instead, the presence of $NaBH_4$ resulted in the inactivation of the enzyme

following a single turnover event due to covalent modification of the active site Pro-1. This observation is consistent with a mechanism where the hydration of **9** proceeds by the formation of a covalent intermediate between enzyme and Pro-1 followed by hydrolysis of the enamine or the imine tautomer to yield acetoacetate (**10**) (Scheme 5).[13] By analogy, the hydration of **2** (or **3**) could proceed to some extent by this route. (The incubation of *cis*-CaaD and **9** for 5 minutes followed by the addition of $NaBH_4$ enabled the determination of the stereochemistry at C-2 of **10**).[13]

Cg10062 processes the alternative substrate **9** with kinetic parameters very similar to those observed for **9** and *cis*-CaaD.[13] However, a stereochemical analysis of Cg10062 and **9** uncovered two differences between the enzymes. First, Cg10062 does not show any loss of activity with **9** in the presence of $NaBH_4$. This observation implies that Cg10062 processes **9** by a direct hydration mechanism rather than via a covalent intermediate. Second, the stereochemical analysis using Cg10062 and **9** showed that it exhibits stereoselective proton addition at C-2 of **9**, but mostly with the opposite stereochemistry (*S*).

The stereochemical analysis indicates that proton transfer to C-2 (of **9**) occurs on opposite sides. Despite the similar active sites (Figure 8) and comparable K_M values, it appears that the allene substrate (i.e., **9**) binds in different orientations in the two enzymes (if the same group provides the proton in both enzymes). The binding mode in *cis*-CaaD favors covalent catalysis, whereas the one is Cg10062 does not. The most significant difference between the two active sites is the composition of the active site loop regions. As such, the loop might be responsible for the different stereochemical results, if it closes in on the active site upon the binding of **9** in the active site of *cis*-CaaD.

The mechanistic and stereochemical experiments with the T34A mutant of *cis*-CaaD lend further support for loop involvement. The mutant is irreversibly inactivated in the presence of **9** and $NaCNBH_3$, like that observed for *cis*-CaaD. However, complete inactivation of the mutant enzyme requires 5 equivalents of substrate per enzyme monomer, indicating that multiple turnovers occur prior to the formation of a covalent intermediate. This suggests that direct enzymatic hydration of the substrate is favored a majority of the time (~80%), and that the T34A mutant is more Cg10062-like. This potential shift in the mechanism of *cis*-CaaD upon mutation may also reflect the corresponding reduction in substrate affinity (Table 2) or a shift in the pK_a value of Pro-1. The mutation does not change the stereochemical outcome, suggesting that the allene binds in the same orientation in the T34A mutant as it does for wild type.

The docking studies provide further insight. The results indicate that **2** binds to *cis*-CaaD ~2 kcal/mol more tightly than it does to Cg10062, as assessed by the energy scoring function of Autodock Vina.[25] This result is consistent with the significantly higher K_m value determined experimentally for the kinetically equivalent substrate **3** and Cg10062 (~110 mM, Table 1) vs *cis*-CaaD (0.16 mM, Table 1). As noted earlier, the physical significance of K_m is difficult to interpret. However, it can be described as the turnover rate divided by the effective rate of substrate binding.[24] Using this definition, the differences in K_m (between *cis*-CaaD and Cg10062) might be explained by the larger active site volume of Cg10062, which could accommodate alternative binding modes (Figure 8). These unproductive binding modes could reduce the rate of effective substrate binding and result in a higher value of K_m. In fact, the docking result for **2** and Cg10062 actually predicts that there are two binding modes with equivalent affinity: one is oriented as shown in Figure 8B and the other is rotated 180°, placing the C3 atom towards the “front” of the active site and away from the active site Pro-1. Such a binding position would likely be non-productive and could account for the higher K_m observed for **3** with Cg10062. In contrast, the results with *cis*-CaaD indicated that such a binding orientation would be energetically unfavorable due to

steric clashes with the loop residue Thr-34. Crystal structure inspection also indicates that the active site volume differences between both enzymes largely reflect the nature of the amino acid at position 34 (Figure 8). In light of these results, it seems reasonable to propose that the reduction in substrate affinity exhibited by the T34A *cis*-CaaD mutant could be due to a corresponding increase in active site volume, thus rendering it more like Cg10062 (see Table 1). The predicted binding mode of **2** in *cis*-CaaD places the carboxylate moiety of that substrate within hydrogen bonding distance of the hydroxyl group of Thr-34. Hence, removing this hydrogen bond could reduce the binding affinity of the substrate.

The results for the T34A mutant of *cis*-CaaD are consistent with a shift in mechanism upon mutation. An in-depth global kinetic analysis (see ref 13) of the *cis*-CaaD loop mutants and Cg10062, including both steady-state and pre-steady state data, is currently being pursued to resolve the remaining mechanistic questions and more clearly define the role of the loop residues in the mechanisms of these enzymes. The results are forthcoming.

Supplementary Material

Refer to Web version on PubMed Central for supplementary material.

Acknowledgments

The protein mass spectrometry analysis was conducted in the Institute for Cellular and Molecular Biology Protein and Metabolite Analysis Facility at the University of Texas at Austin. We thank Steve D. Sorey (Department of Chemistry, University of Texas at Austin) for his expert assistance in the acquisition of the ^{1}H NMR spectra and Hector Serrano for conducting preliminary kinetic experiments with 2,3-butadienoate (**9**). The stopped-flow and rapid-quench-flow instruments and KinTek Explorer data analysis software were provided by KinTek Corp. (Austin, TX).

This research was supported by the National Institutes of Health Grant GM-65324 (CPW) and a fellowship award (F32 GM089083) from the National Institute of General Medical Sciences to G.K.S.

ABBREVIATIONS

Ap	ampicillin
CHMI	5-(carboxymethyl)-2-hydroxymuconate isomerase
CaaD and *cis*-CaaD	*trans*- and *cis*-3-chloroacrylic acid dehalogenase, respectively
ESI-MS	electrospray ionization mass spectrometry
IC	ion chromatography
Kn	kanamycin, LB, Luria-Bertani
MIF	macrophage migration inhibition factor
4-OT	4-oxalocrotonate tauotmerase
PCR	polymerase chain reaction
rmsd	root-mean-square deviation
SDS-PAGE	sodium dodecyl sulfate-polyacrylamide gel electrophoresis
MSAD	malonate semialdehyde decarboxylase
SSE	sum squared error
TIM	triose phosphate isomerase

References

1. Poelarends GJ, Wilkens M, Larkin MJ, Van Elsas JD, Janssen DB. Degradation of 1,3-dichloropropene by *Pseudomonas cichorii* 170. Appl Environ Microbiol. 1998; 64:2931–2936. [PubMed: 9687453]
2. Van Hylckama Vlieg JET, Janssen DB. Bacterial degradation of 3-chloroacrylic acid and the characterization of *cis*- and *trans*-specific dehalogenases. Biodegradation. 1992; 2:139–150. [PubMed: 1368960]
3. Hartmans S, Jansen MW, Van der Werf MJ, De Bont JAM. Bacterial metabolism of 3-chloroacrylic acid. J Gen Microbiol. 1991; 137:2025–2032. [PubMed: 1720168]
4. Poelarends GJ, Serrano H, Person MD, Johnson WH Jr, Murzin AG, Whitman CP. Cloning, expression, and characterization of a *cis*-3-chloroacrylic acid dehalogenase: Insights into the mechanistic, structural, and evolutionary relationship between isomer-specific 3-chloroacrylic acid dehalogenases. Biochemistry. 2004; 43:759–772. [PubMed: 14730981]
5. Poelarends GJ, Johnson WH Jr, Murzin AG, Whitman CP. Mechanistic characterization of a bacterial malonate semialdehyde decarboxylase: identification of a new activity on the tautomerase superfamily. J Biol Chem. 2003; 278:48674–48683. [PubMed: 14506256]
6. Murzin AG. Structural classification of proteins: New superfamilies. Curr Opin Struct Biol. 1996; 6:386–394. [PubMed: 8804825]
7. Poelarends GJ, Whitman CP. Evolution of enzymatic activity in the tautomerase superfamily: Mechanistic and structural studies of the 1,3-dichloropropene catabolic enzymes. Bioorg Chem. 2004; 32:376–392. [PubMed: 15381403]
8. Poelarends GJ, Veetil VP, Whitman CP. The chemical versatility of the β -α-β fold: catalytic promiscuity and divergent evolution in the tautomerase superfamily. Cell Mol Life Sci. 2008; 65:3606–3618. [PubMed: 18695941]
9. De Jong RM, Bazzacco P, Poelarends GJ, Johnson WH Jr, Kim YJ, Burks EA, Serrano H, Thunnissen AMWH, Whitman CP, Dijkstra BW. Crystal structures of native and inactivated *cis*-3-chloroacrylic acid dehalogenase. Structural basis for substrate specificity and inactivation by (*R*)-oxirane-2-carboxylate. J Biol Chem. 2007; 282:2440–2449. [PubMed: 17121835]
10. Guo Y, Serrano H, Johnson WH Jr, Ernst S, Hackert ML, Whitman CP. Crystal structures of native and inactivated *cis*-3-chloroacrylic acid dehalogenase: Implications for the catalytic and inactivation mechanisms. Bioorg Chem. 2011; 39:1–9. [PubMed: 21074239]
11. Robertson, BA. Corynebacterium glutamicum. University of Texas; Austin: 2007. Evolution and divergence in the tautomerase superfamily: A pre-steady state kinetic analysis of *cis*-3-chloroacrylic acid dehalogenase and an inhibition study of its homologue, Cg10062.
12. Robertson BA, Schroeder GK, Jin Z, Johnson KA, Whitman CP. Pre-steady-state kinetic analysis of *cis*-3-chloroacrylic acid dehalogenase: Analysis and implications. Biochemistry. 2009; 48:11737–11744. [PubMed: 19856961]
13. Schroeder GK, Johnson WH Jr, Huddleston JP, Serrano H, Johnson KA, Whitman CP. Reaction of *cis*-3-chloroacrylic acid dehalogenase with an allene substrate, 2,3-butadienoate: hydration via an enamine. J Am Chem Soc. 2012; 134:293–304. [PubMed: 22129074]
14. Poelarends GJ, Serrano H, Person MD, Johnson WH Jr, Whitman CP. Characterization of Cg10062 from *Corynebacterium glutamicum*: Implications for the evolution of *cis*-3-chloroacrylic acid dehalogenase activity in the tautomerase superfamily. Biochemistry. 2008; 47:8139–8147. [PubMed: 18598055]
15. Robertson BA, Johnson WH Jr, Lo HH, Whitman CP. Inactivation of Cg10062, a *cis*-3-chloroacrylic acid dehalogenase homologue in *Corynebacterium glutamicum*, by (*R*)- and (*S*)-oxirane-2-carboxylate: analysis and implications. Biochemistry. 2008; 47:8796–8803. [PubMed: 18646866]
16. Serrano, H. Characterization of the activities of trans-3-chloroacrylic acid dehalogenase and cis-3-chloroacrylic acid dehalogenase and malonate semialdehyde decarboxylase homologues: Mechanism and evolutionary implications. University of Texas; Austin: 2009.

17. Wang SC, Person MD, Johnson WH Jr, Whitman CP. Reactions of *trans*-3-chloroacrylic acid dehalogenase with acetylene substrates: consequences of and evidence for a hydration reaction. Biochemistry. 2003; 42:8762–8773. [PubMed: 12873137]
18. Wang SC, Johnson WH Jr, Czerwinski RM, Whitman CP. Reactions of 4-oxalocrotonate tautomerase and YwhB with 3-halopropiolic acids: analysis and implications. Biochemistry. 2004; 43:748–758. [PubMed: 14730980]
19. Eglinton G, Jones ERH, Mansfield GH, Whiting MC. Acetylenic compounds. XLV. The alkaline isomerization of but-3-ynoic acid. J Chem Soc. 1954:3197–3200.
20. Sambrook, J.; Fritsch, EF.; Maniatis, T. Molecular Cloning: A Laboratory Manual. 2. Cold Spring Harbor Laboratory; Cold Spring Harbor, NY: 1989.
21. Waddell WJ. A simple ultraviolet spectrophotometric method for the determination of protein. J Lab Clin Med. 1956; 48:311–314. [PubMed: 13346201]
22. Laemmli UK. Cleavage of structural proteins during the assembly of the head of bacteriophage T4. Nature. 1970; 227:680–685. [PubMed: 5432063]
23. Johnson KA, Simpson ZB, Blom T. Global Kinetic Explorer: A new computer program for dynamic simulation and fitting of kinetic data. Anal Biochem. 2009; 387:20–29. [PubMed: 19154726]
24. Johnson, KA. Transient-state kinetic analysis of enzyme reaction pathways. In: Sigman, DS., editor. The Enzymes. 3. Academic Press; San Diego: 1992. p. 1-61.
25. Trott O, Olson AJ. AutoDock Vina: improving the speed and accuracy of docking with a new scoring function, efficient optimization, and multithreading. J Comput Chem. 2010; 31:455–461. [PubMed: 19499576]
26. DeLano, WL. The PyMol Molecular Graphics System. DeLano Scientific; San Carlos, CA: 2002.
27. Seeliger D, Groot BL. Ligand docking and binding site analysis with PyMOL and Autodock/Vina. J Comput-Aided Mol Des. 2010; 24:417–422. [PubMed: 20401516]
28. Baas BJ, Zandvoort E, Wasiel AA, Quax WJ, Poelarends GJ. Characterization of a newly identified mycobacterial tautomerase with promiscuous dehalogenase and hydratase activities reveals a functional link to a recently diverged *cis*-3-chloroacrylic acid dehalogenase. Biochemistry. 2011; 50:2889–2899. [PubMed: 21370851]
29. Poelarends GJ, Saunier R, Janssen DB. *trans*-3-Chloroacrylic acid dehalogenase from *Pseudomonas pavonaceae 170* shares structural and mechanistic similarities with 4-oxalocrotonate tautomerase. J Bacteriol. 2001; 183:4269–4277. [PubMed: 11418568]
30. De Jong RM, Brugman W, Poelarends GJ, Whitman CP, Dijkstra BW. The X-ray structure of *trans*-3-chloroacrylic acid dehalogenase reveals a novel hydration mechanism in the tautomerase superfamily. J Biol Chem. 2004; 279:11546–11552. [PubMed: 14701869]
31. Subramanya HS, Roper DI, Dauter Z, Dodson EJ, Davies GJ, Wilson KS, Wigley DB. Enzymatic ketonization of 2-hydroxymuconate: specificity and mechanism investigated by the crystal structures of two isomerases. Biochemistry. 1996; 35:792–802. [PubMed: 8547259]
32. Taylor AB, Johnson WH Jr, Czerwinski RM, Li HS, Hackert ML, Whitman CP. Crystal structure of macrophage migration inhibitory factor complexed with (*E*)-2-fluoro-*p*-hydroxycinnamate at 1.8 Å resolution: implications for enzymatic catalysis and inhibition. Biochemistry. 1999; 38:7444–7452. [PubMed: 10360941]
33. Johnson KA, Simpson ZB, Blom T. FitSpace Explorer: An algorithm to evaluate multidimensional parameter space in fitting kinetic data. Anal Biochem. 2009; 387:30–41. [PubMed: 19168024]
34. Malabanan MM, Amyes TL, Richard JP. A role for flexible loops in enzyme catalysis. Curr Opin Struct Biol. 2010; 20:702–710. [PubMed: 20951028]
35. Richard JP. A paradigm for enzyme-catalyzed proton transfer at carbon: triosephosphate isomerase. Biochemistry. 2012; 51:2652–2661. [PubMed: 22409228]
36. Desai BJ, Wood BM, Fedorov AA, Fedorov EV, Goryanova B, Amyes TL, Richard JP, Almo SC, Gerlt JA. Conformational changes in orotidine 5′-monophosphate decarboxylase: A structure-based explanation for how the 5′-phosphate group activates the enzyme. Biochemistry. 2012; 51:8665–8678. [PubMed: 23030629]
37. Vick JE, Gerlt JA. Evolutionary potential of $(\beta/\alpha)_8$-barrels: stepwise evolution of a “new” reaction in the enolase superfamily. Biochemistry. 2007; 51:8665–8678.

38. Rakus JF, Fedorov AA, Fedorov EV, Glasner ME, Hubbard BK, Delli JD, Babbitt PC, Almo SC, Gerlt JA. Evolution of enzymatic activities in the enolase superfamily: L-rhamnonate dehydratase. Biochemistry. 2008; 47:9944–9954. [PubMed: 18754693]

39. Gerlt JA, Babbitt PC, Jacobson MP, Almo SC. Divergent Evolution in enolase superfamily for assigning functions. J Biol Chem. 2012; 287:29–34. [PubMed: 22069326]

40. Nguyen HH, Wang L, Huang H, Peisach E, Dunaway-Mariano D, Allen KN. Structural determinants of substrate recognition in the HAD superfamily member D-*glycero*-D-*manno*-heptose-1,7-bisphosphate phosphatase (GmhB). Biochemistry. 2010; 49:1082–1092. [PubMed: 20050614]

41. Alber T. Mutational effects on protein stability. Annu Rev Biochem. 1989; 58:765–798. [PubMed: 2673021]

42. Wells JA. Additivity of mutational effects in proteins. Biochemistry. 1990; 29:8509–8517. [PubMed: 2271534]

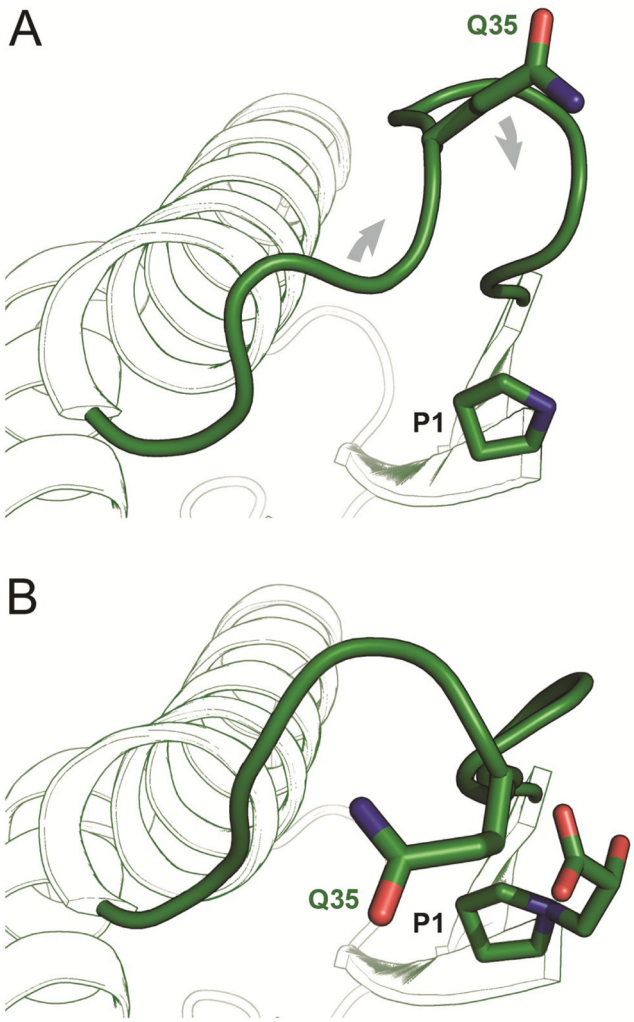

Figure 1.

An active site loop of *cis*-CaaD shown in solid green (Thr-32 to Phe-37) for the apo enzyme (**A**) adopts (gray arrows) a more 'closed' conformation following covalent modification of the active site Pro-1 residue (**B**) (PDB codes 3MF8 and 3MF7, respectively). The loop residue Gln-35 is shown for comparative purposes.

Figure 2.

Sequence alignment of *cis*-CaaD with five selected homologues containing all six catalytically critical residues and >40% sequence similarity: Cg10062 from *C. glutamicum*: NP_599314.1; DiOT from *Desulfurispirillum indicum* S5: YP_004113436.1 [putative 4-OT]; MaCCD from *Marinobacter adhaerens* HP15: ADP98628.1; MsCCD from *Mycobacterium smegmatis* strain MC2 155: YP_887666.1 [OrfY[4]/MsCCH1[28]]; MiCCD from *Mycobacterium intracellulare* ATCC 13950: ZP_05227338.1. The last three entries are annotated as putative *cis*-3-chloroacrylic acid dehalogenases. For clarity, only partial sequences are shown.

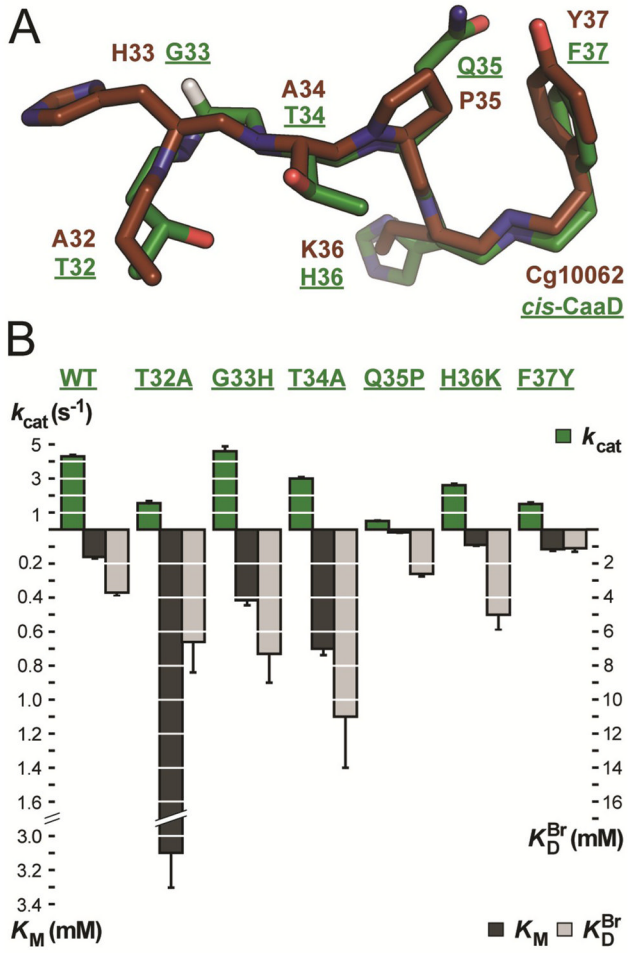

Figure 3.

Graphical summary of loop mutations and corresponding kinetic parameters. (**A**) Structural overlay of the active site loop regions of Cg10062 (brown) and *cis*-CaaD (green) (PDB codes 3N4G and 2FLZ, respectively). (**B**) Bar graph delineating k_{cat} (green), K_m (dark gray) and K_D^{Br} (light gray) for wild-type *cis*-CaaD and the mutants implied in **A**.

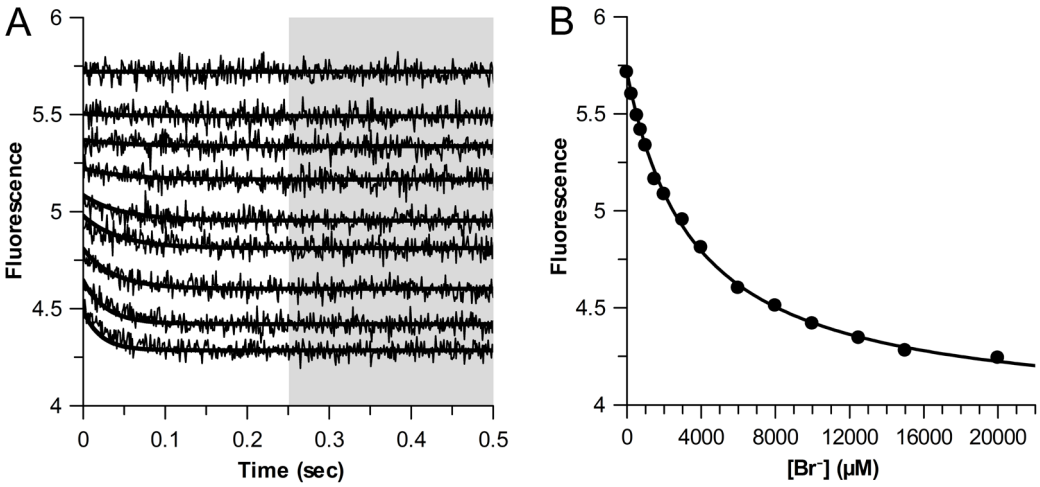

Figure 4.

Stopped-flow fluorescence data for wild-type *cis*-CaaD with increasing bromide concentration (**A**) globally fit by simulation (solid lines) using the kinetic model in Scheme 4. (**B**) A plot of the corresponding steady-state fluorescence endpoints (shaded area) versus bromide concentration fit to eq 1 (solid line).

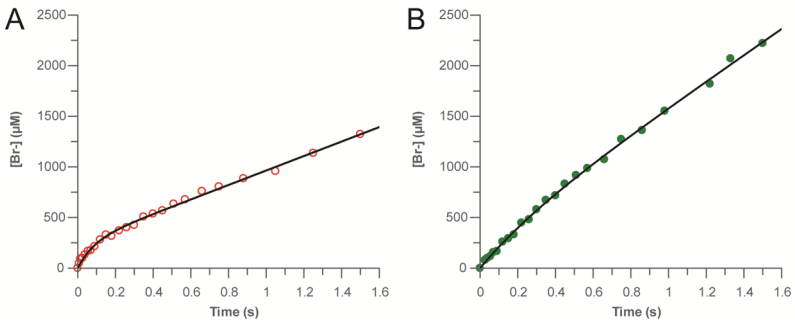

Figure 5.

Rapid quench experiments for the reaction of **3** (10 mM after mixing) with both wild-type *cis*-CaaD (**A**) and T34A *cis*-CaaD (**B**). The solid line shown represents a fit of the pre-steady state burst of bromide formation to eq 2, yielding burst rates (λ) of 12 ± 2 and 3 ± 1 s^{-1}, respectively.

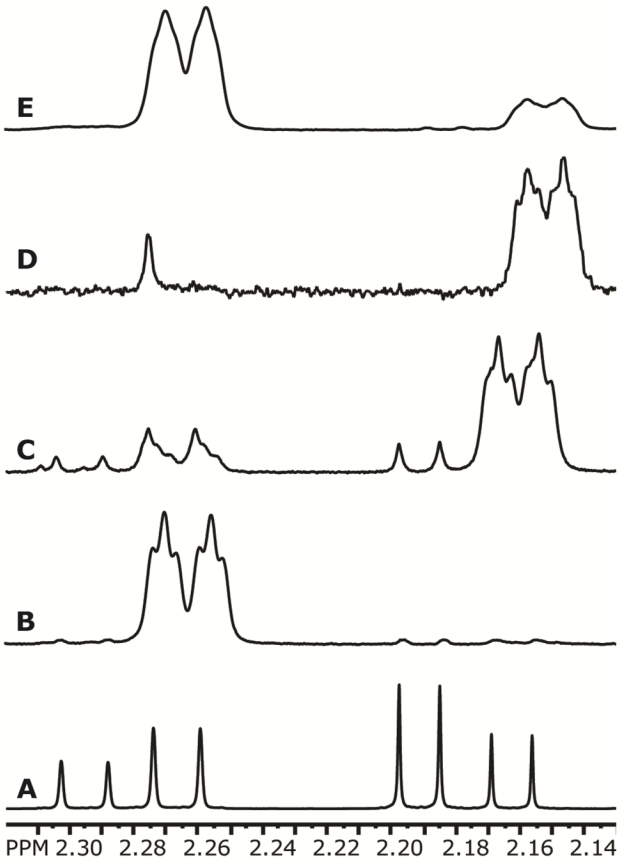

Figure 6.

^{1}H NMR spectrum (500 MHz) in D_2O of (A) fully protio (3*S*)-**11**, (B) (2*S*,3*S*)-[2-D]**11** generated as reported elsewhere[13], (C) (2*R*,3*S*)-[2-D]**11** derived from the *cis*-CaaD-catalyzed hydration of **9** in D_2O[13], (D) (2*R*,3*S*)-[2-D]**11** derived from the T34A-*cis*-CaaD-catalyzed hydration of **9** in D_2O (see text), and (E) (2*S*,3*S*)-[2-D]**11** derived from the Cg10062-catalyzed hydration of **9** in D_2O (see text). The signal at 2.275 in spectrum D is generated by an unknown contaminant. The spectra shown in A–C are reproduced from reference 13.

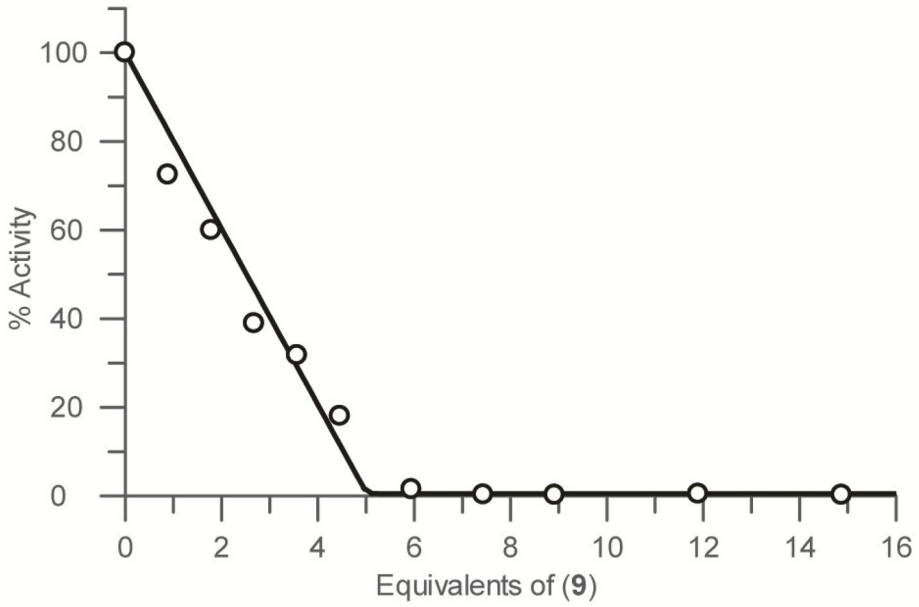

Figure 7.

The remaining T34A *cis*-CaaD activity (%) plotted as a function of increasing equivalents of **9** (per monomer) in the presence of $NaCNBH_3$ at pH 8. Data were fit (solid line) to a modified form of the quadratic equation (see text and Supporting Information Text S1).

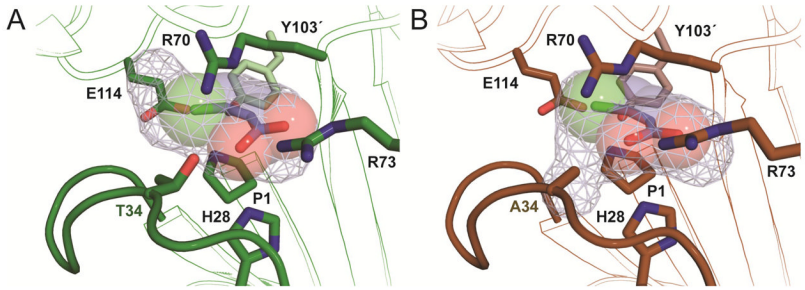

Figure 8.

In silico docking results representing the best fit for **2** to *cis*-CaaD in green (**A**) and Cg10062 in brown (**B**) (PDB codes 2FLZ and 3N4G, respectively). Both docked ligands, shown as space-filling models, fit within the active site volume of each enzyme, as represented by the mesh surfaces (gray). The loop residue at position 34 is also included for comparative purposes.

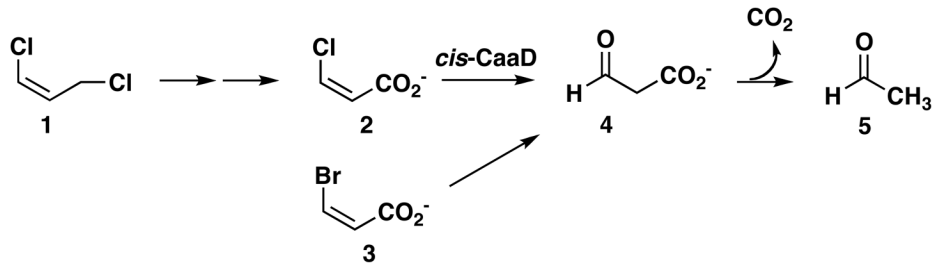

Scheme 1.
The last two steps in the catabolic pathway for *cis*-1,3-dichloropropene in *P. pavonaceae* 170.

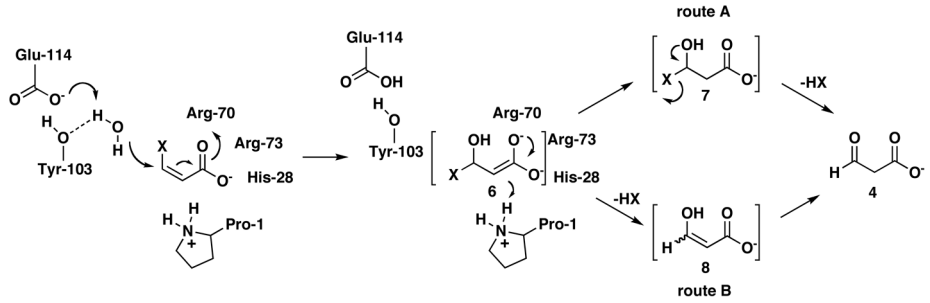

Scheme 2.
The proposed mechanism for *cis*-CaaD with the key amino acids identified.

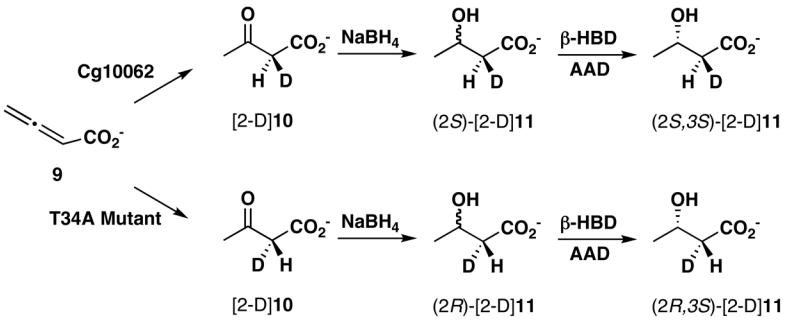

Scheme 3.

The conversion of **9** to [2-D-**10**] by Cg10062 and the T34A mutant of *cis*-CaaD in D_2O, and the subsequent analysis of the stereochemistry at C-2.

Scheme 4.
Kinetic model for binding of product bromide.

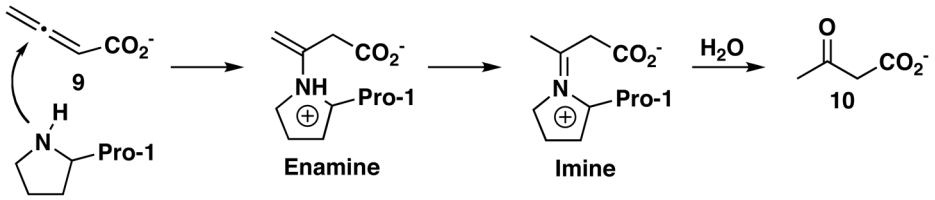

Scheme 5.

An alternative mechanism for the *cis*-CaaD-catalyzed conversion of **9** to **10** involving a covalent intermediate.

Table 1

Steady-state kinetic parameters for the hydrolytic dehalogenation of **3** and bromide dissociation constants determined for wild-type *cis*-CaaD, *cis*-CaaD mutants, and Cg10062.

	k_{cat} (s^{-1})	K_M (μM)	k_{cat}/K_M (M^{-1} s^{-1})	$K_D^{Bromide}$ (μM)	ΔF^c
cis-CaaD[a]	4.3 ± 0.1	160 ± 10	2.7×10^4	3700 ± 200	−1.8 ± 0.05
T32A[b]	1.5 ± 0.1	3100 ± 200	3.9×10^2	6600 ± 1800	−0.8 ± 0.08
G33H[a]	4.6 ± 0.3	415 ± 30	1.1×10^4	7300 ± 1700	−1.3 ± 0.10
T34A[b]	3.0 ± 0.1	700 ± 40	4.3×10^3	11000 ± 3000	−0.6 ± 0.07
Q35P[a]	0.5 ± 0.01	16 ± 2	3.1×10^4	2600 ± 150	−2.5 ± 0.04
H36K[a]	2.6 ± 0.1	90 ± 5	2.9×10^4	5000 ± 900	−2.4 ± 0.13
F37Y[a]	1.5 ± 0.1	115 ± 10	1.3×10^4	1100 ± 200	−1.2 ± 0.05
Cg10062[b]	3.0 ± 0.5	110000 ± 20000	2.7×10^1	3800 ± 400	−0.3 ± 0.02

[a] Steady-state kinetic parameters were determined by following the decrease in UV absorbance at 224 nm (see text).

[b] *Steady*-state kinetic parameters were determined by the coupled assay (see text).

[c] Difference between the initial fluorescence and the final predicted fluorescence saturation value (see eq 1).

Table 2

Steady-state kinetic parameters for enzyme-catalyzed hydration of **9**.[a]

Enzyme	K_M (μM)	k_{cat} (s^{-1})	k_{cat}/K_M ($M^{-1}s^{-1}$)
cis-CaaD[b]	690 ± 30	6 ± 0.1	8.7×10^3
T34A *cis*-CaaD[c]	7500 ± 1100	8 ± 1	1.1×10^3
Cg10062[d]	780 ± 130	4 ± 0.3	5.1×10^3

[a] The kinetic parameters were measured in 100 mM Na_2HPO_4 buffer (pH 8) at 22 °C. Errors are standard deviations.

[b] Values taken from ref 13.

[c] Steady-state kinetic parameters were determined by following the decrease in UV absorbance at 255 nm (see text).

[d] Steady-state kinetic parameters were determined by following the decrease in UV absorbance at 224 nm (see text).